Analysis of the Variability in the Raindrop Size Distribution and Its Effect on Attenuation at 20–40 GHz

Adrian Justin Townsend, Robert J. Watson, *Member, IEEE*, and Duncan David Hodges

***Abstract*—A key problem in determining the level of attenuation from the rainfall rate is the considerable variability in the raindrop size distribution. This letter investigates the effects of the variability of the raindrop size distribution (DSD) on the estimation of specific attenuation. Disdrometer data from three sites in the U.K. were analyzed to derive the three parameters (D_m, μ, and N_w) of the normalized gamma distribution. The statistics of the parameters were analyzed as a function of time of year and rainfall intensity. From the raindrop size distribution data, the impact on attenuation at 20–40 GHz was investigated. A simple model to quantify the uncertainty of the raindrop size distribution has been created. Finally, we have shown qualitatively that differences between measured and modeled attenuation can partly be explained by uncertainty in the raindrop size distribution. Furthermore, we also show that although the model for mean attenuation is relatively constant, the standard deviation is much more variable even for sites in close proximity.**

***Index Terms*—Attenuation, radio propagation meteorological factors, rain, satellite communication.**

I. Introduction

CURRENT frequency allocations below Ku-band are becoming increasingly congested [1]. The problem continues to grow as the use of satellite communications becomes more popular. In order to compensate for increase in demand, satellite operating frequencies have to be raised to deliver larger channel capacity. However, raising the operating frequency has the adverse result of intensifying the attenuation effects of the troposphere [2]. At high frequencies such as V-band, despite the effects of cloud, rain remains the dominant cause of attenuation.

To maintain a high-quality satellite service, fade mitigation techniques can be implemented to compensate for effects such as rain and cloud [3]. Prediction of signal fade can greatly improve the implementation and effectiveness of fade mitigation techniques [1]. Therefore, it is important to be able to predict rain fade accurately.

The aim of this letter is to quantify the uncertainty in the calculation of rain attenuation for a given rainfall rate. The ITU-R uses a single, on-average fit to represent all raindrop size distributions, while other models such as Leitao–Watson [4] use two rain types representing widespread and convective rain. The attenuation calculation can be improved through a better understanding of the variability of the raindrop size distribution and its effects since rain attenuation is a function of raindrop size distribution.

Manuscript received August 21, 2009. First published November 03, 2009; current version published November 17, 2009. This work was supported by the EPSRC.

The authors are with the Department of Electrical and Electronic Engineering, University of Bath, Bath BA2 7AY, U.K. (e-mail: A.J.Townsend@bath.ac.uk; R.J.Watson@bath.ac.uk; eepddh@bath.ac.uk).

Digital Object Identifier 10.1109/LAWP.2009.2035724

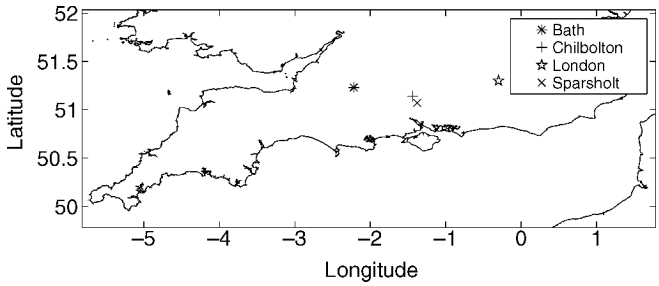

Fig. 1. Map of the U.K. showing disdrometer locations (Bath to Chilbolton ≈80 km; Chilbolton to Sparsholt ≈7.5 km).

II. Disdrometer Data Analysis

The raindrop size distribution (DSD) is the number of drops m^3/mm over different raindrop sizes. This can be used to calculate the rainfall rate and radio wave attenuation.

Two Joss–Waldvogel disdrometers were used to measure DSDs at Chilbolton, U.K. $(51°14\ \mathrm{N}, 1°44\ \mathrm{W})$, and Sparsholt, U.K. $(51°07\ \mathrm{N}, 1°38\ \mathrm{W})$, over five years from 2003–2007. A third optical disdrometer (Thies Clima Laser Precipitation Monitor) was used at the University of Bath, Bath, U.K. $(51°23\ \mathrm{N}, 2°22\ \mathrm{W})$, to obtain further two years of data from 2007–2008. The DSD from each disdrometer can be written as [5]

$$N(D_i) = \frac{N_A(D_i)}{A_r T v(D_i) \Delta D_i} \tag{1}$$

where $N_A(D_i)$ is the number of drops measured in the drop-size class, D_i is average raindrop diameter of the drop-size class (mm), A_r is the measurement area of the disdrometer (m^2), T is the time interval for one measurement (s), $v(D_i)$ is the fall velocity of the drop (ms^{-1}), and ΔD_i is the bin-width of each drop-size class. In this letter, we consider the time interval to be 1 min. This is a compromise between observing the rain dynamics versus reducing the uncertainty in the DSD.

An analytical distribution was fitted to all the measured DSDs in order to define the parameters of the distribution. Various analytical forms have been suggested such as Marshall and Palmer (exponential) and Ulbrich (gamma-shaped DSD). In this work,

the normalized gamma distribution is considered, which is defined by three parameters and written as [6]

$$N(D) = N_w \cdot \frac{6}{4^4} \cdot \left[\frac{(4+\mu)^{(4+\mu)}}{\Gamma(4+\mu)}\right] \cdot \left(\frac{D}{D_m}\right)^{\mu} \cdot \exp\left[-(4+\mu)\cdot\frac{D}{D_m}\right] \quad (2)$$

where N_w, μ, and D_m define the normalized gamma distribution and D is the drop size. Following the approach of [5], a normalized gamma distribution was fitted to measured DSDs using a maximum likelihood method to determine μ and the method of moments to calculate N_w and D_m.

The rainfall rate and attenuation were calculated for each DSD. Rainfall rate (R in mm/h) can be written as

$$R = \frac{3.6}{10^3} \cdot \frac{\pi}{6} \cdot \int_0^{\infty} v(D) D^3 N(D) dD \quad (3)$$

where $v(D)$ is the fall velocity of the drop at diameter D. Specific attenuation (A in dB/km) can be calculated as

$$A = 4.343 \times 10^3 \cdot \int_0^{\infty} Q_t(D) N(D) dD \quad (4)$$

where Q_t is the total extinction cross section, calculated using the T-matrix method [7], with the drop-shape model of Chuang and Beard [8].

III. Results

To study the variability of the DSD as a function of rainfall rate and time of the year, the data was partitioned into seasons: Spring (March, April, May), Summer (June, July, August), Autumn (September, October, November), and Winter (December, January, February). The data were analyzed to determine any patterns in the DSD parameters. Histograms of D_m, μ, and N_w were determined for rainfall rates between 0 and 30 mm/h in intervals of 1 mm/h.

As an example, Figs. 2–4 show the histograms of the normalized gamma DSD parameters as a function of rainfall rate. From Fig. 2, it can be seen that D_m generally increases with increasing rainfall rate. The variability of D_m also increases with rainfall rate. Similar patterns are seen for D_m in all seasons. It can be seen that no clear pattern is observed for μ. The N_w parameter shows significant variation at lower rainfall rates, but tends toward the value suggested by Marshall–Palmer at higher rainfall rates (larger than 10 mm/h). The distributions for N_w and μ show more variability. Examination of Figs. 2–4 shows that qualitatively there are two regions delineated at approximately 10 mm/h. The two regions likely represent the transition between stratiform and convective rain.

Our analysis has considered frequencies from 20 to 40 GHz. However, the figures presented in this paper are at 20.7 GHz because of available beacon data for validation. Fig. 5 shows the variability in the attenuation rainfall relationship for the five years worth of data from Chilbolton, U.K.

Since we are interested in the variability in the estimation of attenuation from rainfall rate, it is instructive to analyze histograms of attenuation conditioned on rainfall rate interval rather than just scatter plots. As an example, Fig. 6 shows normalized histograms of specific attenuation at 20.7 GHz conditioned on rainfall rates between 5–6 mm/h and 15–16 mm/h for

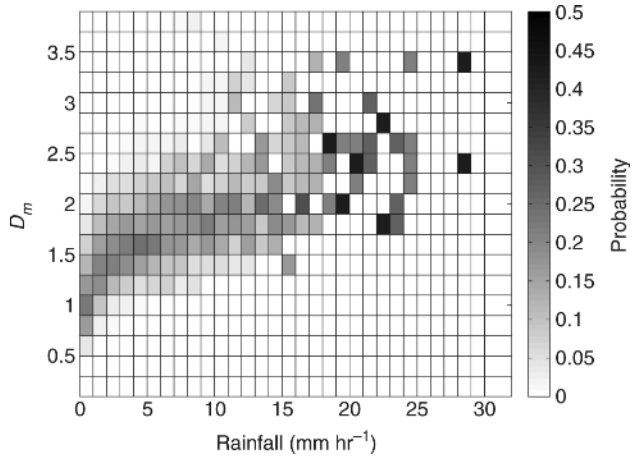

Fig. 2. Normalized gamma parameter D_m probability histograms versus rainfall rate during Spring months (Chilbolton).

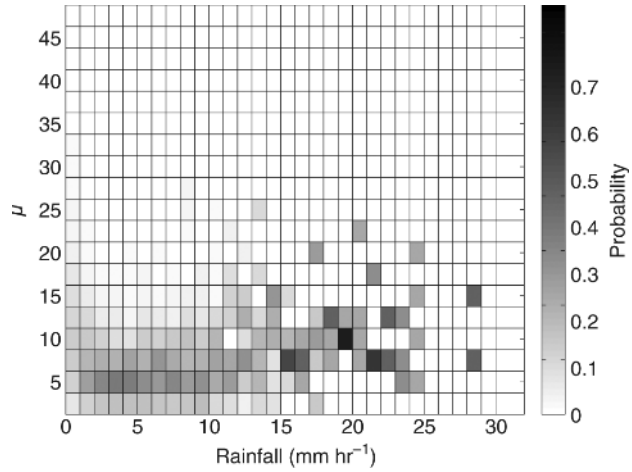

Fig. 3. Probability histograms of parameter μ over rainfall rate during the Spring (Chilbolton).

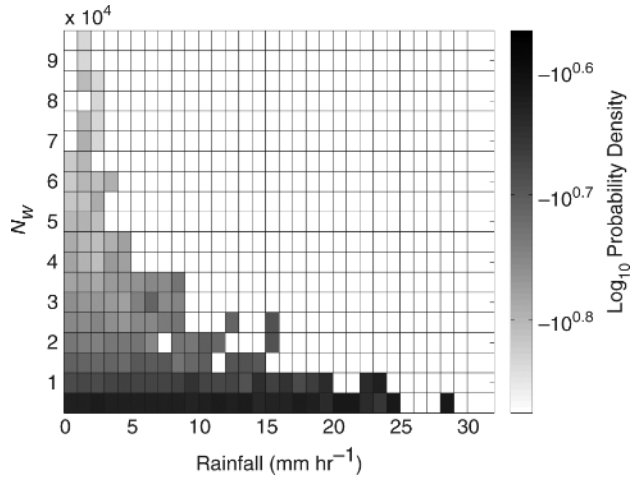

Fig. 4. Probability density histograms of parameter N_w over rainfall rate during the Spring (Chilbolton).

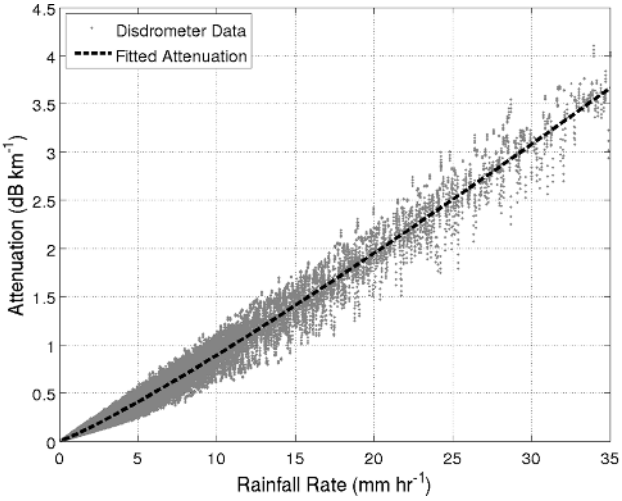

Fig. 5. Attenuation versus rainfall rate for all disdrometer data at Chilbolton (frequency $= 20.7$ GHz).

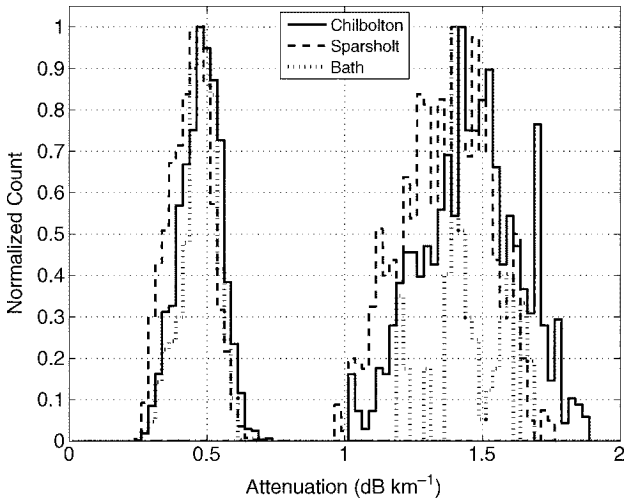

Fig. 6. Examples of normalized specific attenuation histograms for rainfall rate 5–6 mm/h (left-hand side) and 15–16 mm/h (right-hand side) at 20.7 GHz for Bath, Chilbolton, and Sparsholt.

the three sites based on attenuation bin-widths of 0.025 dB/km. It can be seen that there is general agreement between the mean values and the shapes of the distributions between sites. The histograms for other rainfall rates are of similar shape and can be approximated by a Gaussian distribution. For rainfall rates between 0 and 30 mm/h, the mean and the variance of the attenuation histograms were determined. This rainfall rate range was selected as it is representative of 99.99% of rainfall for most of the U.K. Furthermore, this interval also ensures a statistically significant number of data points at the highest rainfall rates.

A power-law relationship was fitted to the mean $(\overline{A})$ and standard deviation (σ_A) of the data as follows:

$$\overline{A} = aR^b, \quad \sigma_A = cR^d \tag{5}$$

where $(\overline{A})$ is the fitted attenuation, a and b are coefficients determined by the power-law fit, (σ_A) is the fitted standard deviation, and c and d are coefficients determined by the power law fit to the standard deviation.

Figs. 7 and 8 show the mean and standard deviation, respectively, of the histogram fits as a function of rainfall rate. It can be seen that there is good agreement between the means, but the standard deviation shows significantly more scatter (as illustrated from the differences in the shape of the histograms in Fig. 6). Although the difference in scatter can be partially explained by instrument differences at the sites, it does indicate the possibility of climatic differences affecting the variability of the DSD even for small separation distances (Chilbolton–Bath ≈80 km; Sparsholt–Chilbolton ≈7.5 km). As expected the means agree well with the ITU-R P.838-2. The fit to the mean effectively represents a least-squares fit to the data. Similar analysis was performed at 30 and 40 GHz, again with the mean showing good agreement with the ITU-R. Table I summarizes the power-law coefficients for the fits.

To consider the effect of the DSD variability on earth–space link attenuation, we have compared link attenuation from the Global Broadcast Satellite (GBS) beacon measurements at Chilbolton to attenuation estimated from disdrometer rainfall rate data. The GBS is a geostationary satellite with a beacon at 20.7 GHz. The rain height was estimated 0.36 km above the 0°

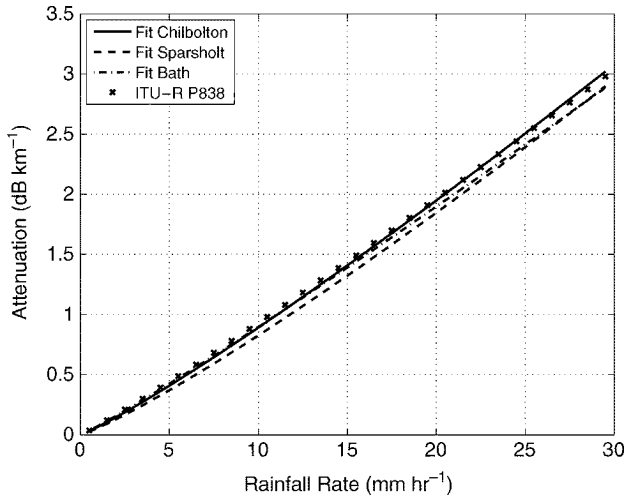

Fig. 7. Mean specific attenuation at 20.7 GHz against rainfall rate for fitted estimates of attenuation, Chilbolton histogram attenuation, and the ITU-R.

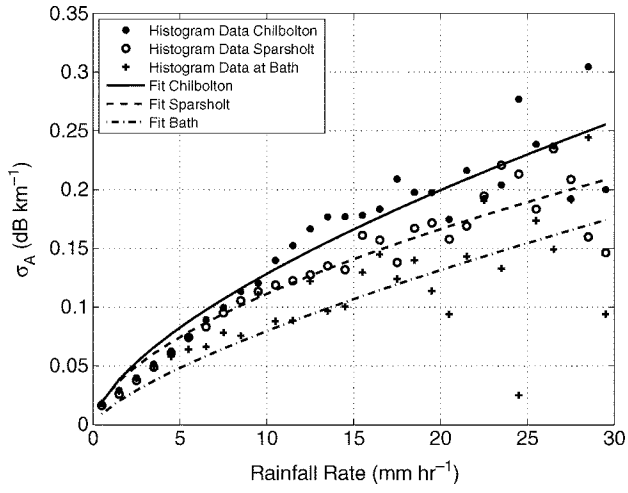

Fig. 8. Fitted attenuation standard deviation versus rainfall rate at 20.7 GHz at Chilbolton, Sparsholt, and Bath.

TABLE I
CURVE-FITTED PARAMETERS FOR CALCULATING MEAN SPECIFIC ATTENUATION ($\overline{A} = aR^b$ FOR R $= 0 - 30$ mm/h) AND STANDARD DEVIATION ($\sigma_A = cR^d$ for R $= 0 - 30$ mm/h)

Frequency (GHz)	Mean						Standard Deviation					
	Bath		Chilbolton		Sparsholt		Bath		Chilbolton		Sparsholt	
	a	b	a	b	a	b	c	d	c	d	c	d
20.7	0.0746	1.08	0.0664	1.13	0.0572	1.16	0.0293	0.58	0.0297	0.64	0.0151	0.72
30	0.1617	1.02	0.1701	1.04	0.1494	1.07	0.0567	0.12	0.0599	0.41	0.0765	0.19
40	0.2838	0.96	0.3500	0.94	0.3224	0.97	0.0384	0.66	0.0186	1.14	0.0194	1.03

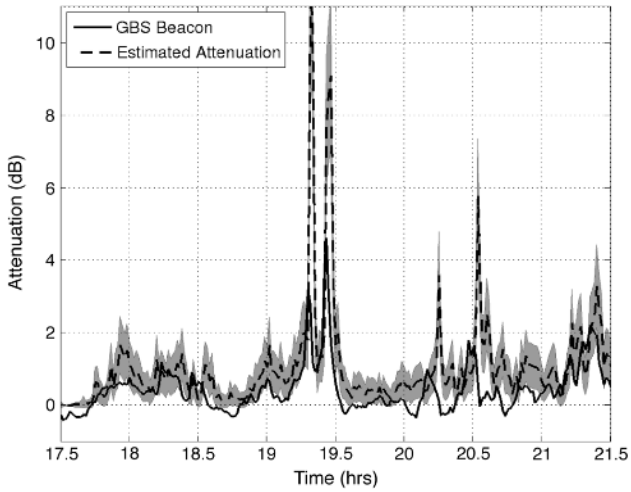

Fig. 9. Chilbolton GBS beacon and estimated satellite signal attenuation at 20.7 GHz versus time, where shaded region shows $\pm\sigma_A$.

isotherm determined from surface temperature measurements close to the link and the disdrometer using a temperature lapse rate of 6.5 K/km. The ITU-R P.618-8 effective path length model was used to scale the specific attenuation to yield the link attenuation.

Fig. 9 shows typical link attenuation measured from the GBS beacon and the estimated link attenuation based on rainfall rate determined from the disdrometer on June 22, 2004. Note that the link attenuation was estimated from rainfall only, ignoring the raindrop size distribution data available from the disdrometer. The small negative excursions are remnants of the beacon post-processing required since the GBS satellite is in an inclined geosynchronous orbit ($\approx 4^\circ$) [9]. The shaded region shown represents ± 1 standard deviation above and below the mean of the estimated attenuation. This area shows the uncertainty in attenuation that could be expected due to variability in the DSD alone. It can be seen that although there is some disagreement between the GBS beacon and mean attenuation the data is generally bounded within the shaded region. The occasions where this is not the case generally correspond to low attenuation and may be due to the different sampling volumes of the two measurements, variation in the rain height, or incorrect attenuation baseline determination.

IV. CONCLUSION

Twelve years of drop size distribution data from three sites has been examined. The normalized gamma distribution parameters N_w and D_m show some patterns with rainfall rate and season. However, the shape parameter μ is not well correlated with rainfall rate. The impact of the variability of the drop size distribution on attenuation is dependent on both season and rainfall intensity. Although there are undoubtedly other effects the differences between measured and estimated slant path-attenuations, these can be potentially explained by variability of the raindrop size distribution.

Further work will consider how the parameters of the raindrop size distribution could be estimated or at least constrained by other meteorological information, such as temperature, pressure gradients, and wind speed. Such data is available from, for example, numerical weather prediction models. This approach could be integrated into propagation prediction schemes and fade mitigation techniques. In its simplest form, this could merely be a classifier between stratiform and convective rain. A more elaborate scheme might attempt to estimate numerical values of the DSD parameters.

ACKNOWLEDGMENT

The authors thank Rutherford Appleton Laboratory and the British Atmospheric Data Centre for the disdrometer and beacon data.

REFERENCES

[1] A. D. Panagopoulos, P. D. M. Arapoglou, and P. G. Cottis, "Satellite communications at Ku, Ka, and V bands: Propagation impairments and mitigation techniques," *IEEE Commun. Surveys Tutorials*, vol. 6, no. 3, pp. 2–14, 2004.

[2] B. R. Arbesser-Rastburg and A. Paraboni, "European research on Ka-band slant path propagation," *Proc. IEEE*, vol. 85, no. 6, pp. 843–852, 1997.

[3] L. Castanet, "Fade mitigation techniques for new satcom systems at Ka and V Bands," Ph.D. dissertation, Dept. Electromagnetism and Radar, SUPAERO Univ., Toulouse, France, 2001.

[4] M. J. Leitao and P. A. Watson, "Method for prediction of attenuation on earth-space links based on radar measurements of the physical structure of rainfall," *Proc. IEEE*, vol. 133, no. 4, pp. 429–441, 1986.

[5] M. Montopoli, F. S. Marzano, and G. Vulpiani, "Analysis and synthesis of raindrop size distribution time series from disdrometer data," *IEEE Trans. Geosci. Remote Sens.*, vol. 46, no. 2, pp. 466–478, Feb. 2008.

[6] J. Testud, S. Oury, R. A. Black, P. Amayenc, and X. Dou, "The concept of "normalized" distribution to describe raindrop spectra: A tool for cloud physics and cloud remote sensing," *J. Appl. Meteorol.*, vol. 40, pp. 1118–1140, 2001.

[7] P. W. Barber and S. C. Hill, *Light Scattering by Particles: Computational Methods*. Singapore: World Scientific, 1990.

[8] C. C. Chuang and K. V. Beard, "A numerical model for the equilibrium shape of electrified raindrops," *J. Atmospheric Sci.*, vol. 47, no. 11, pp. 1374–1389, 1990.

[9] D. D. Hodges and R. J. Watson, "An analysis of conditional site diversity: A study at ka-band," *IEEE Trans. Antennas Propag.*, vol. 57, no. 3, pp. 721–727, Mar. 2009.